fractal and fractional

Article

Driver Training Based Optimized Fractional Order PI-PDF Controller for Frequency Stabilization of Diverse Hybrid Power System

Guoqiang Zhang [1], Amil Daraz [1,2,*], Irfan Ahmed Khan [3], Abdul Basit [1,2], Muhammad Irshad Khan [4] and Mirzat Ullah [5]

1 School of Information Science and Engineering, NingboTech University, Ningbo 315100, China
2 College of Information Science and Electronic Engineering, Zhejiang University, Hangzhou 310027, China
3 Department of Electrical Engineering, Faculty of Engineering, Universiti Malaya, Federal Territory of Kuala Lumpur 50603, Malaysia
4 College of Electronics and Information Engineering, Nanjing University of Aeronautics and Astronautics (NUAA), Nanjing 210000, China
5 Graduate School of Economics and Management, Ural Federal University, Yekaterinburg 620002, Russia
* Correspondence: amil.daraz@nbt.edu.cn

Abstract: This work provides an enhanced novel cascaded controller-based frequency stabilization of a two-region interconnected power system incorporating electric vehicles. The proposed controller combines a cascade structure comprising a fractional-order proportional integrator and a proportional derivative with a filter term to handle the frequency regulation challenges of a hybrid power system integrated with renewable energy sources. Driver training-based optimization, an advanced stochastic meta-heuristic method based on human learning, is employed to optimize the gains of the proposed cascaded controller. The performance of the proposed novel controller was compared to that of other control methods. In addition, the results of driver training-based optimization are compared to those of other recent meta-heuristic algorithms, such as the imperialist competitive algorithm and jellyfish swarm optimization. The suggested controller and design technique have been evaluated and validated under a variety of loading circumstances and scenarios, as well as their resistance to power system parameter uncertainties. The results indicate the new controller's steady operation and frequency regulation capability with an optimal controller coefficient and without the prerequisite for a complex layout procedure.

Keywords: renewable energy resources; optimization techniques; fractional order controller; power system; load frequency control; heuristic techniques; driver training-based optimization

check for updates

Citation: Zhang, G.; Daraz, A.; Khan, I.A.; Basit, A.; Khan, M.I.; Ullah, M. Driver Training Based Optimized Fractional Order PI-PDF Controller for Frequency Stabilization of Diverse Hybrid Power System. *Fractal Fract.* **2023**, *7*, 315. https://doi.org/10.3390/fractalfract7040315

Academic Editors: António Lopes, Behnam Mohammadi-Ivatloo and Arman Oshnoei

Received: 3 March 2023
Revised: 28 March 2023
Accepted: 2 April 2023
Published: 6 April 2023

1. Introduction

Electrical power has played a significant role in technological development for many years. The demand for electricity has greatly increased because of population growth and related technological advancements. Conventional, non-renewable energies led to energy sector installations in the past. However, because of their dearth and unfavorable effects on the environment, concerns are shifting away from these sources and toward the installation of renewable energy-based sources (RESs) [1]. To replace non-renewable supplies with RESs, such as wind energy, photovoltaic (PV) generation, biodiesel, etc., it is necessary to put more emphasis on sustainable development. Additionally, the use of energy storage devices to improve green energy-based power grids and the collaborative management of installed electric cars have drawn significant interest from researchers, businesses, and governmental incentives and regulations. They may contribute to maintaining the robustness and dependability of electricity grids [2]. Furthermore, by using modern single/multi-constraint optimization methods, such as stochastic optimization [3] and resilient optimization approaches [4], the performance of the power sector can be improved. Renewable-based power grids must overcome several obstacles, including intermittency, decreased inertia, irregular loading patterns, etc. The connectivity of grids powered by renewable energy is advantageous in several ways. However, renewable energies bring about unstable electricity grids that respond poorly to disturbances [5]. When compared to typical grids that are non-renewable-based, the poor inertial response is the main reason for power grid instability. The inability of photovoltaic and wind generation to sustain a significant inertial response results from their interaction with power interface converters, which restricts their ability to balance power demands [6]. Low inertial responses cause severely unbalanced power grids and lower flexibility of harmonic distortion in renewable-based power grids when renewable penetration level increases [7].

The literature contains several study recommendations for incorporating electrical vehicles (EVs) into the power system [8,9]. Green transportation has become a challenging issue with the current load equilibrium techniques, however, due to the complexity of managing a networked, multi-area system. The literature has suggested several integrated orders, predictive models, fuzzy logic controllers, neural networks, fractional orders, and advanced control systems as the best controllers for load frequency control (LFC) [10–12]. The tilt, derivative, proportional, integrator, and filter derivative have all been extensively linked in the literature to create several LFC systems. The PI regulator was introduced for EVs in [13]. However, stability issues with this controller exist, specifically when the time delay (TD) is taken into account. The filter-based tilt integral derivative controller for hybrid power networks has been optimized using the differential evolution algorithm, which was presented in [13]. The PI, TD, and filter controller parameters were combined to analyze the power networks in [14]. A hybrid approach using an updated form of particle swarm optimization (PSO) and the genetic algorithm was reported in [15] for establishing the controller employed to stabilize the frequency of power networks. An imperialist competitive search (ICA) method with a fractional order controller has been suggested in [16] for multi-generational networks. The stated controller can successfully enhance the performance of the power technique when there are several step variations in the production and/or loading. In two-area power networks, the FOPID and FLC are cascaded to accomplish frequency regulation [17]. Additionally, it has been suggested to use the grey wolf optimization algorithm to develop the load frequency controller multi-generation power networks [18].

The FOPID with FO filter was suggested by the authors in [19], and the SCA technique was utilized to successfully improve the controller parameters. The authors of [20] utilized an algorithm known as Harris hawk's optimization to design the P-I based LFC parameters in the best possible way. With the addition of capacitive energy storage, Daraz et al. exploited FOTIDN for multisource IPS while taking into account various non-linearities [21]. By using a hybrid of SCA and fitness-dependent algorithms, the parameters of the suggested method are changed. The authors in [22] used control EVs with TID controllers and optimized bee colony heuristics to change the settings of the suggested controller. The virtual inertia monitoring approach reported in [23] was expanded using PSO. In [24], an ultra-capacitor energy storage device has been developed to address AGC issues in connected PS. An improved design for the FOTID controller has also been provided using the path finder optimization technique [25]. Amil et al. recommended fine-tuned MFOPID/FOPID controllers for a hybrid system in [26], utilizing the jellyfish search algorithm. The authors in [27] proposed a different method of using the imperialist competitor optimizer to find the ideal settings of the second-order proposed controller for frequency stabilization systems. A modified tilt derivative with a filter controller based on fractional order is presented by Mohamed et al. in [28] and has been tuned using the artificial hummingbird optimizer technique. The salp swarm algorithm was introduced in [29] to tune the gains of PID controllers considering two area networks. Additionally, the dual-stage controller was developed in [30] using the butterfly optimization approach. A unique cascaded FO-ID with filter controller is suggested for AGC systems in PS with wind/solar/fuel systems in the study mentioned in [31].

It is now clear that the literature has a variety of LFC concepts that employ various optimization methods. The combination of the LFC-type and the selected optimizer greatly affects how well the power grid performs during transients. To lessen the projected loading impacts of RESs in future low-inertial grids, however, enhanced LFC method performance and design approaches are needed. This paper first introduces a cascaded structure, FOI, and PD with filter regulators in order to develop a revolutionary modified FO LFC method. From a different angle, their parameters need a lot of work to be adjusted. Several meta-heuristic optimization techniques lack reliability because of their greater inclination to settle at local minimums [32]. Correct tuning is also required for a variety of parameters, especially for FO-based LFC methods. The decision to optimize the parameters is therefore fraught with difficulty [33]. Extended delay times, exhaustion, sensitivity, and selectivity to parameter changes are other issues that certain optimizers face. Another issue with some optimizers is their lengthy processing periods, which require numerous iterations to ensure solution convergence. This study introduces driver training-based optimization (DTBO), a new stochastic optimization technique that imitates the human activity of driving training. The DTBO design was primarily influenced by how people learn to drive in driving schools and by instructor-training programs. Three stages of the proposed algorithm are mathematically modeled: (1) instruction from the driving coach, (2) modeling of student behavior after instructor techniques, and (3) practice. The effectiveness of DTBO is assessed using 23 common objective functions, including unimodal, multimodal, and IEEE CEC(2017) test function types [34]. The suggested algorithm has a number of benefits for difficult optimization challenges as well as its anticipated versatility in handling many types of optimization problems, given that many problems require more flexibility than DTBO can provide. Due to its mathematical foundation, this algorithm can be used to address a variety of engineering optimization problems, especially those with high dimensionality. Based on the inspiration given by the current gap in LFCs and their layout techniques, the study's main contributions are summarized below:

- For the connected PS taking into account electrical vehicles, a novel cascade structure of the proportional integral (PI)-proportional derivative with filter (PDF) is adopted.
- The proposed cascaded control structure is compared to a number of other control approaches, such as PIDF, PID, and PI controllers.
- The performance of the suggested LFC technique is enhanced using driver–teacher-based optimization (DTBO), which optimally selects the parameters of the suggested controller. The outcomes of DTBO are contrasted with those of other contemporary meta-heuristic algorithms, including the ICA and JSO.
- To ensure the viability of the system, a variety of non-linearities, such as time delay (TD), governor dead zone (GDZ), boiler dynamic (BD), and generation rate limitations (GRL), have been examined for the proposed hybrid power system.
- A synchronized participation of EVs with current-generating power units is offered using the proposed FOPI-PDF central controller.
- Finally, utilizing load changes of $\pm 25\%$ and $\pm 50\%$ and system parameters within a $\pm 40\%$ tolerance, the suggested cascaded controller's robustness is verified.

2. Power System Investigation

The suggested FOPI-PDF controller's design is shown in Figure 1, employing the two area-connected PS with the selected EVs and RESs. The RESs are placed in all of the areas, with solar energy in region 1 and wind energy in area 2. Area 1 comprises a reheat thermal plant, whereas area 2 holds the hydro generation unit. Furthermore, it is presumed that both regions have an equal distribution of EVs. The scheme is built in Matlab/Simulink using the PS information from [35], which is presented in Appendix A. Additionally, the physical limitations of PS, including GRL and GDZ, are taken into consideration by using the GRL rate (0.003 and 0.0017 pu/s), allowing for non-linearity and a more precise thermal unit analysis. Likewise, hydro power plants have a maximum production rate of 0.045 pu/s for increasing rates and 0.06 p.u. for declining rates [36–38].

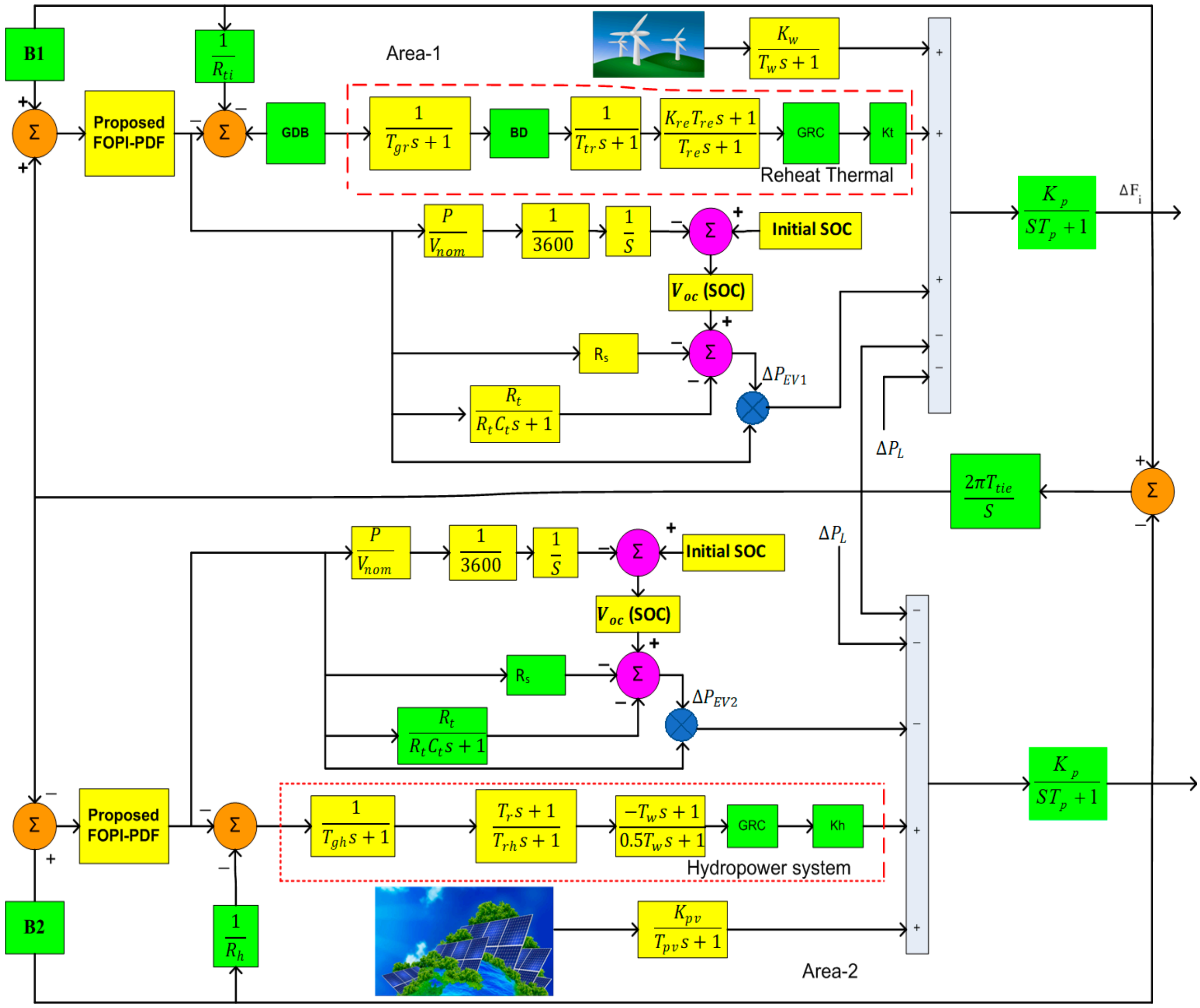

Figure 1. Transfer function model of hybrid power system.

The transfer function (TF) given in Equation (1) represents the governor dead zone (GDZ) with a margin of 0.50% [39].

$$\frac{\text{GDZ}}{\text{GDB}} = \frac{N_1 + N_2 s}{T_{sg}s + 1} \tag{1}$$

where N_1 = 0.8 and,

$$\text{N}_2 = \frac{-0.2}{\pi} \tag{2}$$

Time delay (TD) can influence controller implementation, which can amplify oscillations in the system. Consequently, this work contains a dynamic simulation that considers TD in the controller error field as well as various operational nonlinearities. Figure 2 denotes the transfer function typical for the BD. This paradigm can be used to assess both inefficiently managed gas/oil-fired power units as well as efficiently managed coal-fired power units. When the boiler regulator senses a change in pressure/steam flow rate, the pertinent controls are instantly initiated. This is how traditional steam power plants change their production. Equation (3) is an illustration of the TF boiler dynamics concept [39,40].

$$T_{cpu}(s) = \frac{K_{1b}(1+T_{1b}s)(1+T_{rb}s)}{(1+0.1T_{rb}s)s} \tag{3}$$

$$T_f(s) = \frac{e^{-t_d(s)}}{Ts+1} \tag{4}$$

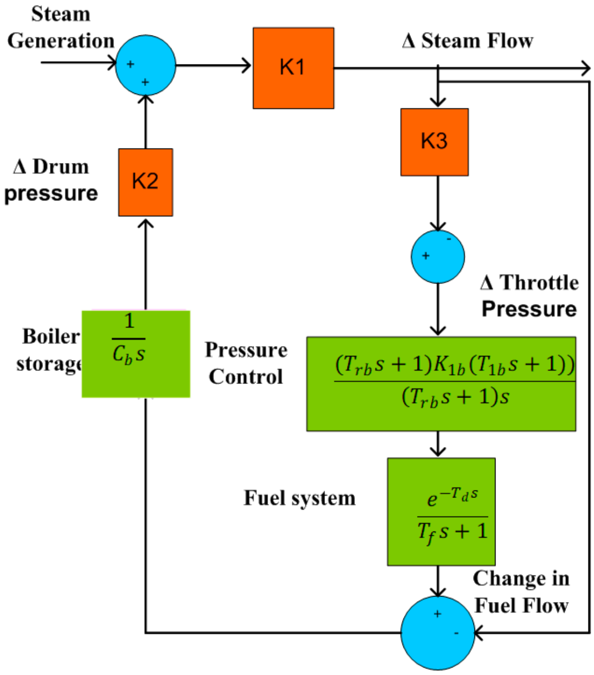

Figure 2. Drum type structure of boiler dynamics.

2.1. Modeling of Conventional Power Systems

The general TF model for the thermal reheat unit ($GT(s)$), which is represented by Equations (5)–(8) correspondingly, includes the reheat ($G_{T1}(s)$), turbine ($G_{T2}(s)$), and governor ($G_{T3}(s)$).

$$G_{T1}(s) = \frac{1+T_{re}K_{re}\mathrm{s}}{(1+T_{re}\mathrm{s})} \tag{5}$$

$$G_{T2}(s) = \frac{1}{(1+T_{tr}\mathrm{s})} \tag{6}$$

$$\mathrm{G}_{T3}(\mathrm{s}) = \frac{1}{(1+\mathrm{T_{gr}s})} \tag{7}$$

$$\mathrm{G}_T(\mathrm{s}) = \frac{1+T_{re}K_{re}\mathrm{s}}{(1+T_{gr}\mathrm{s})(1+T_{re}\mathrm{s})(1+T_{tr}\mathrm{s})} \tag{8}$$

Likewise, Equations (9)–(12), respectively, reflect the total TF of the hydropower system ($GH(s)$) in addition to the TF of the droop compensation ($G_{H1}(s)$), TF of the hydro governor ($G_{H2}(s)$, and TF of the penstock with turbine ($G_{H3}(s)$).

$$G_{H1}(s) = \frac{(1-T_w\mathrm{s})}{(1+0.5T_w\mathrm{s})} \tag{9}$$

$$G_{H2}(s) = \frac{(1+T_{rs}\mathrm{s})}{(1+T_{rh}\mathrm{s})} \tag{10}$$

$$G_{H3}(s) = \frac{1}{\left(1 + T_{gh}s\right)} \tag{11}$$

$$G_H(s) = \frac{(1 - T_w s)(1 + T_{rs}s)}{\left(1 + T_{gh}s\right)(1 + 0.5T_w s)(1 + T_{rh}s)} \tag{12}$$

2.2. Renewable Energy Resources (RES,s) Modelling

The following models are used to express the $G_{PV}(s)$ of a solar energy system and $G_w(s)$ of a wind energy system [41]:

$$G_{PV}(s) = \frac{K_{PV}}{T_{PV}s + 1} \tag{13}$$

$$G_w(s) = \frac{K_T}{T_T s + 1} \tag{14}$$

where Kpv and Tpv stand for the PV plant's gain and time constant, respectively. Similarly, K_T and T_T stand for the wind farm's gain and time constant, respectively.

2.3. Modeling of EV Systems

The batteries of today's EVs may successfully regulate the PS performance. In response to electrical system management demands, they can be activated or deactivated. They might also increase the power system's reliability, efficiency, and dynamic response, among other things. Due to the fluctuating pattern of RESs and the associated electrical demands, one significant task of their use is the role of an EV in preserving the system stability of a PS. Figure 3 [42] displays the EV dynamical model that was used for the frequency response analysis in this paper.

The Nernst equation [42] is used in the model to illustrate the relationship between the linked EVs' open circuit voltage (Voc) and state of charge (SOC):

$$\mathrm{V_{oc}(SOC)} = \mathrm{S}\frac{RT}{F}\ln\left(\frac{\mathrm{SOC}}{\mathrm{C_{nom}} - \mathrm{SOC}}\right) + \mathrm{V_{nom}} \tag{15}$$

where $\mathrm{C_{nom}}$ and $\mathrm{V_{nom}}$ are the nominal capacities and voltages of the EV batteries, respectively. R stands for the gasoline constant, F for the Faraday constant, and T for temperature. S stands for the sensitivity parameter.

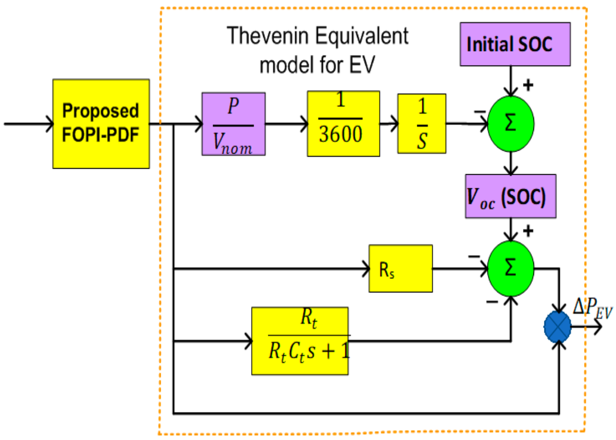

Figure 3. Dynamic model of EV system.

3. Driving Training Based Optimization (DTBO)

DTBO is a new stochastic optimization technique recently proposed in [34] that emulates the human action of driving guidance. The DTBO design was primarily influenced by how people learn to drive in driving schools and by instructor-training programs. Three stages of DTBO are mathematically modeled: (1) instruction from the driving coach, (2) modeling of student behavior after instructor techniques, and (3) practice. The effectiveness of DTBO is assessed using 23 common objective functions, including unimodal, multimodal, and IEEE CEC(2017) test function forms. The suggested DBOA has a number of benefits for difficult optimization challenges as well as its anticipated versatility in handling many types of optimization problems, given that many problems require more flexibility than DTBO can provide. Due to its mathematical foundation, DTBO can be used to address a variety of engineering optimization problems, especially those with high dimensionality. The detail of DTBO algorithm comprises of the subsequent steps:

3.1. Mathematical Representations of DTBO

Driving instructors and students make up the members of the population-based metaheuristic known as DTBO. Members of the DTBO are potential answers to the specified problem, which is depicted using a population matrix in Equation (16). Equation (17) is used to initialize these member positions at random at the beginning of implementation [34].

$$X = \begin{bmatrix} x_{11} & \cdots & x_{ij} & \cdots & x_{im} \\ \vdots & \ddots & \vdots & \ddots & \vdots \\ x_{i1} & \cdots & x_{ij} & \cdots & x_{im} \\ \vdots & \ddots & \vdots & \ddots & \vdots \\ x_{N1} & \cdots & x_{Nj} & \cdots & x_{Nm} \end{bmatrix}_{N\times M} = \begin{bmatrix} X_1 \\ \vdots \\ X_i \\ \vdots \\ X_N \end{bmatrix}_{N\times M} \quad (16)$$

$$x_{i,j} = lb_j + \left(ub_j - lb_j\right) \times \mathrm{r},\ i = 1,\ 2,\ 3\ldots\ldots.N,\ J = 1,\ 2,\ldots,m \quad (17)$$

where N is the population dimension, m denotes the problem of variables, r belongs to a random number between [0, 1], and ub_j and lb_j are the upper and lower bounds, respectively. X is the inhabitants of DTBO, x_i is the ith applicant solution, and $x_{i,j}$ is the value of the jth mutable represented by the ith applicant solution. The objective function's standards are modeled by the vector in Equation (18).

$$F = \begin{bmatrix} F_1 \\ \vdots \\ F_i \\ \vdots \\ F_N \end{bmatrix}_{N\times 1} = \begin{bmatrix} F(X_1) \\ \vdots \\ F(X_i) \\ \vdots \\ F(X_N) \end{bmatrix}_{N\times 1} \quad (18)$$

where F_i is the cost function provided by the ith applicant solution and F denotes the vector of the objective functions. Applicant solutions in DTBO are restructured during the following three steps: (i) beginner driver training by a driving tutor; (ii) beginner driver modeling using tutor skills; and (iii) learner driver rehearsal.

3.2. Phase 1: (Learner Driver Training by a Driving Instructor)

The trainee driver selects the driving instructor in the first phase of the DTBO update, and the instructor then instructs the learner driver in driving. The best members of the DTBO community are divided into trainee drivers and a limited group of driving instructors. Members of the population will go to various locations in the search space after selecting the driving teacher and mastering their techniques. This will strengthen the DTBO's investigation capabilities in the broad quest for and detection of the perfect region. As a result, this stage of the DTBO update illustrates the exploratory capabilities of this algorithm. The N memberships of the DTBO are chosen as driving tutors for an individual rehearsal based on an evaluation of the values of the cost function, as given in Equation (19).

$$DI = \begin{bmatrix} DI_1 \\ \vdots \\ DI_i \\ \vdots \\ DI_{NDI} \end{bmatrix}_{N_{DI} \times m} = \begin{bmatrix} DI_{11} & \cdots & DI_{1i} & \cdots & DI_{1m} \\ \vdots & \ddots & \vdots & \ddots & \vdots \\ DI_{i1} & \cdots & DI_{ij} & \cdots & DI_{im} \\ \vdots & \ddots & \vdots & \ddots & \vdots \\ DI_{N_{DI1}} & \cdots & DI_{N_{DIj}} & \cdots & DI_{N_{\mathrm{DIm}}} \end{bmatrix}_{N_{DI} \times m} \tag{19}$$

where $N_{DI} = \left[0.1 \cdot N \cdot \left(1 - \frac{t}{T}\right)\right]$ is the number of driving tutors, DI is the driving instructor matrix, DI_i is the ith driving teacher, $DI_{i,j}$ is the jth dimension, and T is the maximum number of iterations. The new location for each element in this DTBO phase is first determined using Equation (20) according to the mathematical modeling of this phase. Then, if the new position increases the value of the function, it replaces the old one in accordance with Equation (21).

$$x_{i,j}^{PI} = \begin{cases} x_{i,j} + r \cdot \left(DI_{k_i,j} - I \cdot x_{i,j}\right), \ FDI_{k_i,j} < F_i; \\ x_{i,j} + r \cdot \left(I \cdot x_{i,j} - DI_{k_i,j}\right), \ Otherwise \end{cases} \tag{20}$$

$$X_i = \begin{cases} X_i^{PI}, \ F_i^{PI} < F_i; \\ X_i, \ Otherwise \end{cases} \tag{21}$$

where I and r are random numbers chosen from the range [0, 1] and [1, 2], respectively. DI_{k_i}, is arbitrarily selected from the range [1, 2,..., N_{DI}], that represents a driving instructor, $x_{i,j}^{PI}$ is its jth dimension, F is its objective function value, and X_i^{PI} is the new intended location for the ith applicant solution based on the first stage.

3.3. Phase-2 (Modeling of Student Behavior after Instructor Techniques)

The trainee driver imitates the instructor in this stage by trying to mimic all of the instructor's gestures and driving techniques. This method shifts DTBO participants to several locations within the quest space, boosting the DTBO's exploration capacity. A novel location is created based on the weighted sum of each participant with the teacher in accordance with Equation (22) to mathematically mimic this idea. According to Equation (23), the updated location will replace the prior one if it increases the objective function rate.

$$x_{i,j}^{P2} = P \cdot x_{i,j} + r \cdot (I - P) \cdot DI_{k_i,j} \tag{22}$$

$$X_i = \begin{cases} X_i^{P2}, \ F_i^{P2} < F_i; \\ X_i, \ Otherwise \end{cases} \tag{23}$$

where F_i^{P2} represents the objective function value, X_i^{P2} sis the updated position for i^{th} candidates, $x_{i,j}^{P2}$ represents its jth dimension while the pattern index (P) is denoted by below equation.

$$P = 0.01 + 0.09(I - t/T) \tag{24}$$

3.4. Phase 3 (Practice)

The third stage of the DTBO upgrade is based on each trainee driver's individual practice to strengthen and improve their driving abilities. In this stage, each novice driver aims to get a little bit closer to his best abilities. This phase is set up so that each participant can find a more advantageous position by conducting a local search near where they are currently located. The ability of DTBO to leverage confined pursuit is demonstrated in this step. This DTBO phase is precisely described so that, in accordance with Equation (25), a random position is initially created close to each population member. If this location increases the value of the goal function, Equation (26) states that it should take the place of the prior position.

$$x_{i,j}^{P3} = x_{i,j} + R\cdot(1-2r)\left(1-\frac{t}{T}\right)\cdot x_{i,j} \quad (25)$$

$$X_i = \begin{cases} X_i^{P3}, \ F_i^{P3} < F_i; \\ X_i, \ Otherwise \end{cases} \quad (26)$$

where R is a constant with a value of 0.05. A DTBO iteration is finished after modifying the sample population in accordance with the first through third phases. The algorithm entered the following DTBO iteration with the modified population. Through the maximum number of repetitions, the update procedure is repeated during the mentioned phases and according to Equations (20)–(26). After DTBO has been applied to the provided problem, the best possible choice solution that was noted during execution is presented as the solution. Figure 4 shows the flowchart for the suggested DTBO approach.

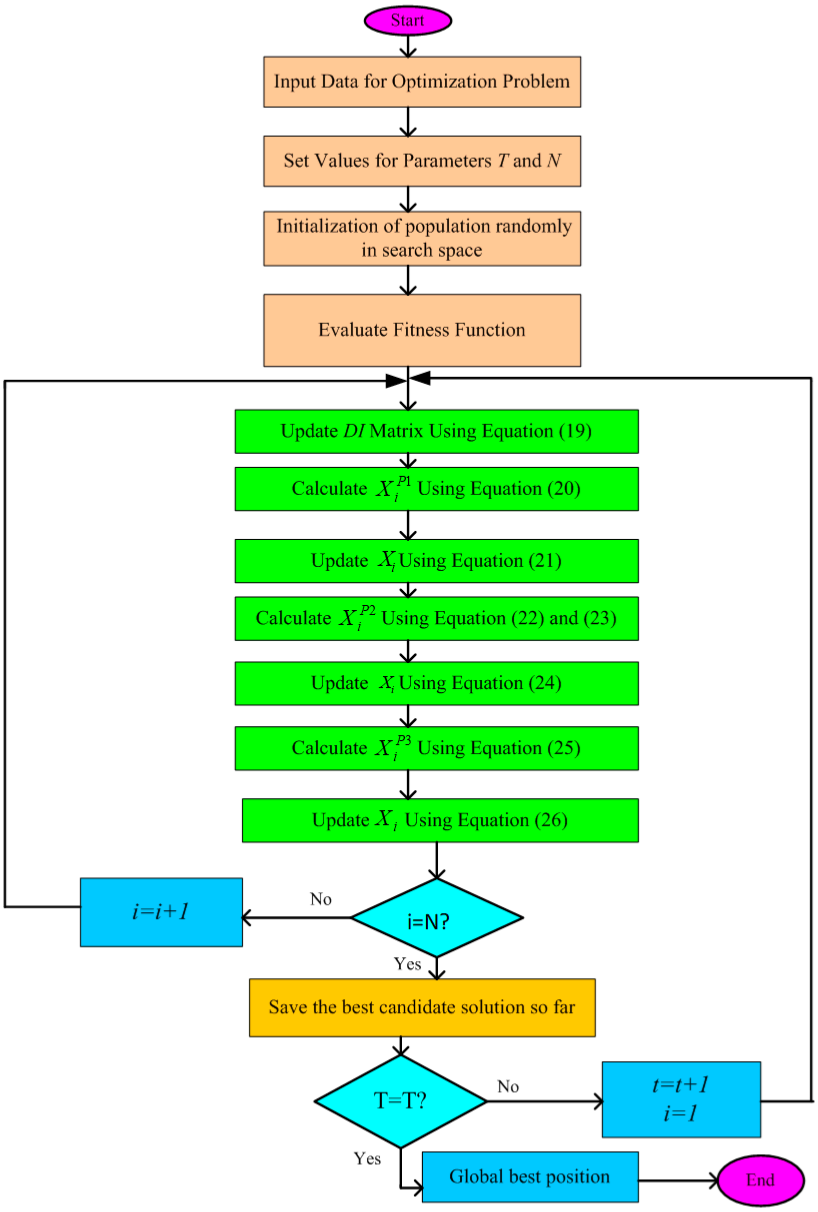

Figure 4. The flowchart for the suggested DTBO approach.

4. Proposed Control Structure and Fitness Function

Traditional PID control can improve controller stability and response time. However, because of the derivative mode, excessive control inputs are injected into the plant. The primary culprit in this problem is the noise that is already present in the control indicators. By including a filtering portion in the derivative part, the inserted noise is removed. The chattering noise can be reduced by fine-tuning the pole [43,44]. As a result, the FOPI-PDF is used in the proposed cascaded controller to improve the effectiveness of the control methodology by combining fractional order integer with proportional and the derivative filter. The transfer function of FOPI, PDF, and FOPIDF is depicted below:

$$C_1(s) = \frac{Y(s)}{R(s)} = K_p + \frac{K_i}{s^\lambda} \tag{27}$$

$$C_2(s) = \frac{Y(s)}{R(s)} = K_P + K_d\left[\frac{N_d s}{s+N_d}\right] \tag{28}$$

$$FOPIDF = \frac{Y(s)}{R(s)} = K_p + \frac{K_i}{s^\lambda} + K_d s^\mu\left[\frac{N_d s}{s+N_d}\right] \tag{29}$$

The schematic diagrams of the *FOPID*, *FOPI-PDF*, and combined controller structures are shown in Figure 5, Figure 6, and Figure 7, respectively. The proposed configuration has the capability to reduce the influence of turbulence on the control system's performance. Equation (30) could also be used to express the primary loop transfer function.

$$Y(s) = G(s)U(s) + d(s) \tag{30}$$

where *G(s)* represents the execution and *U(s)* represents the input pulse. Equation (31) can be used to calculate *U(s)*.

$$U(s) = C_1(s) \cdot C_2(s) \tag{31}$$

The cascaded (*FOPI-PDF*) controller gains will be ascertained by minimizing the cost function (*CF*) using the DTBO algorithm. The integral of time weighted by the squared error (*ITSE*) [4,26] is chosen as the CF because it can reduce time settling and overwhelm high oscillations quickly [30]:

$$ITSE = J = \int_0^t t\left[\Delta F_1^2 + \Delta F_2^2 + \Delta P_{tie}^2\right] dt \tag{32}$$

The following restrictions apply to the proposed FOI-PDN controller gains.

$$K_p^{Min} \le K_p \le K_p^{Max};\ K_d^{Min} \le K_d \le K_d^{Max};\ K_i^{Min} \le K_i \le K_i^{Max};\ \lambda^{Min} \le \lambda \le \lambda^{Max};\ N_d^{Min} \le N_d \le N_d^{Max};\ \mu^{Min} \le \mu \le \mu^{Max} \tag{33}$$

Several studies have shown that the Oustaloup recursive approximation (ORA) of FO derivatives can be implemented in real-time digitally [45]. It has become more familiar to the ORA with regard to the tuning processes involved with FO controllers. Since it is widely used in the literature in order to model the integrals and derivatives of FO, the ORA method has been used in this paper. In mathematical terms, the α^{th} FO derivative (s^α) can be expressed as follows [45]:

$$s^\alpha \approx w_h^\alpha \prod_{K=-N}^{N} \frac{s+\omega_k^z}{s+\omega_k^p} \tag{34}$$

where ω_k^z denotes the zeros and ω_k^p denotes the poles, which can be represented by the below equations, respectively.

$$\omega_k^z = \omega_b \left(\frac{\omega_h}{\omega_b}\right)^{\frac{k+N+\frac{1-\alpha}{2}}{2N+1}} \tag{35}$$

$$\omega_h^{\alpha} = \left(\frac{\omega_h}{\omega_b}\right)^{\frac{-\alpha}{2}} \prod_{k=-N}^{N} \frac{\omega_k^p}{\omega_k^z} \quad (36)$$

The approximate FO operator's function has $(2N + 1)$ zeroes/ poles. ORA filter order is determined by the number N (order = $(2N + 1)$). This paper uses the ORA with ($M = 5$) and a frequency range ($\omega \in [\omega_h, \omega_b]$) of $[10^3, 10^{-3}]$ rad/s.

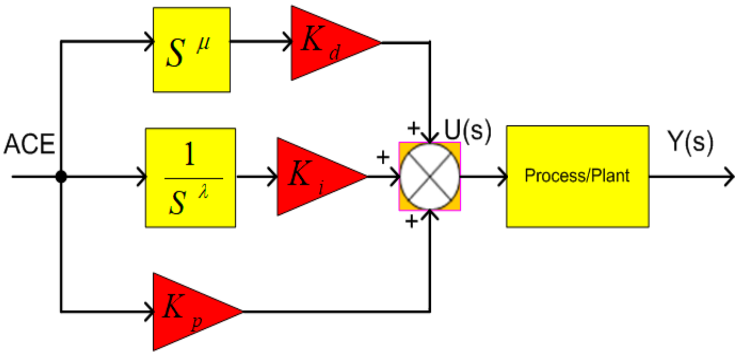

Figure 5. Design of FOPID controller.

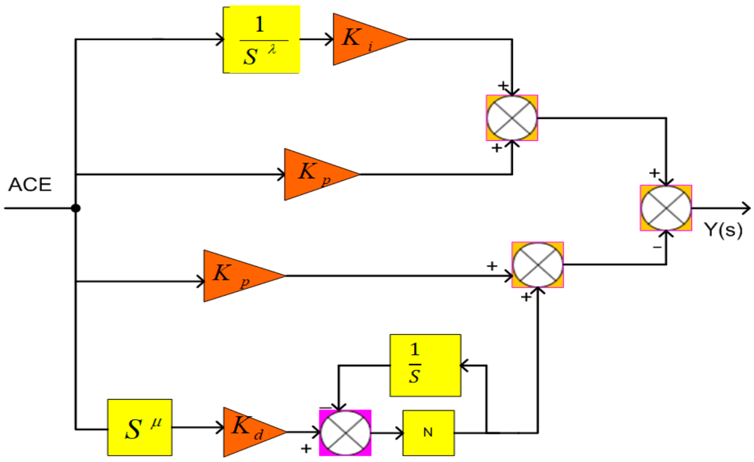

Figure 6. Design of FOPI-PDF controller.

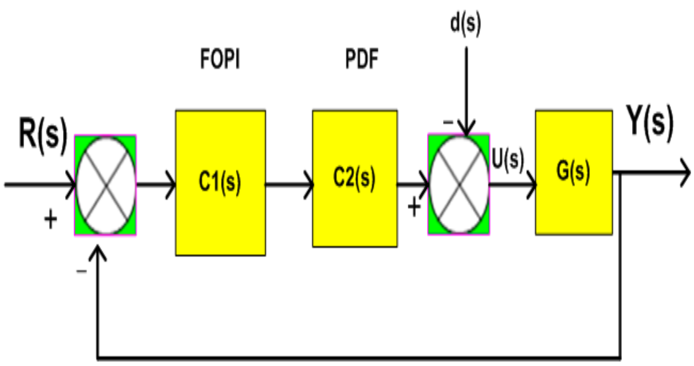

Figure 7. Cascaded form of controller.

5. Implementation, Results and Discussion

This part investigates the efficacy and validity of the unique FOPI-PDF controller implementation, depicted in Figure 1, in conjunction with EVs for enhancing IPS with the LFC problem. To ensure fairness, a newly suggested DTBO method was employed to tune the various control parameters of the FOPI-PDF and other controllers such as the FOPIDF, PI, and PID. The DTBO technique was constructed using the MATLAB program m-file code and linked up with the simulink mechanism of the researched interconnected PS to reach the LFC objective function. Table 1 shows the DTBO-based controller parameters for the given case study after running the optimization algorithms 15 times using the data from Appendix B. The robustness of the proposed FOPI-PDF controller is tested by comparing it to traditional and advanced controllers such as PID, PI, and FOPIDF, using the same alignment as the EV system that uses the DTBO approach. The per unit load change in each case is set at (5%) =0.05 p.u. The following case studies critically evaluate the results obtained from the analyzed multi-area IPS.

Table 1. Optimal values obtained for the proposed techniques.

Parameters	Case-1			Case-2			
	DTBO	**JSO**	**ICA**	**FOPI-PDF**	**FOPIDF**	**PID**	**PI**
K_{p1}	1.998	1.877	1.900	1.098	1.950	1.405	1.893
K_{i1}	1.678	1.458	0.400	1.878	1.340	1.012	1.032
K_{d1}	1.998	1.877	1.200	1.998	0.902	1.405	-
K_{p2}	0.345	0.123	1.145	1.889	-	-	-
λ_1	0.710	0.556	1.620	0.710	0.620	-	-
μ_1	0.671	0.601	1.863	0.671	0.823	-	-
N_1	8.678	3.234	9.972	8.678	9.972	-	9.899
K_{p3}	1.678	1.234	2.000	1.678	2.000	1.232	1.767
K_{d2}	1.998	1.877	1.405	1.998	1.989	1.405	-
K_{p4}	0.644	1.990	1.235	1.009	-	-	-
μ_2	0.710	0.456	0.620	0.710	0.620	-	-
λ_2	0.878	0.972	0.678	0.878	0.678	-	-
N_2	9.900	9.897	7.893	9.900	7.894	-	-

5.1. Case-1

In this case, the effectiveness of the DTBO approach was contrasted with the performances of the JSO, hDE-PS, ICA, and FPA algorithms. As shown in Figure 8a–c, the dynamic response for each optimization algorithm technique has been evaluated for the interconnected tie line (ΔP_{tie}), area 2 (ΔF2), and area 1 (ΔF1). Table 2 shows the overall comparison for (ΔF1), (ΔF2), and (ΔPtie) in terms of maximum overshoot (MO), minimum undershoot (MU), and settling time (ST). Figure 8a–c, demonstrates that the FOPI-PDF controller tuned with the DTBO approaches has improved STs for (ΔPtie) and (ΔF2) of 29.11% and 35.08%, respectively, but almost the same peak overshoot as the FOPI-PDF adjusted with the ICA approaches. Table 2 demonstrates that the DTBO method outperforms the JSO strategies for (ΔF1), (ΔF2), and (ΔPtie) in terms of ST (46.63%, 30.32%, and 14.11%) and MU (79.12%, 73.99%, and 90.00%). When compared to an JSO approach, the DTBO algorithm reduced peak overshoot by 70.11%, 78.12%, and 69.01% when taking into account (ΔF1), (ΔF2), and (ΔPtie), respectively. For the interconnected tie line (ΔPtie), area 2 (ΔF2), and area 1 (ΔF1), it is evident from Table 2 that our suggested DTBO algorithm outperforms JSO, ICA, hDE-PS [42], hTLBO with PS [10], and FPA [25] techniques.

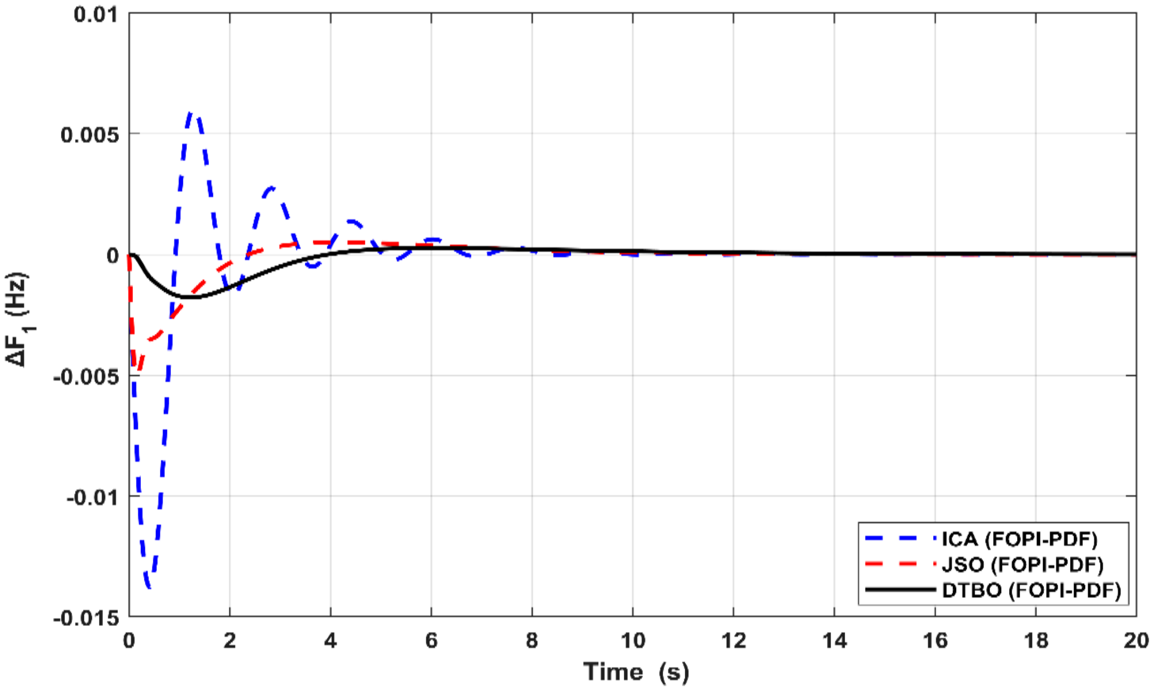

(**a**)

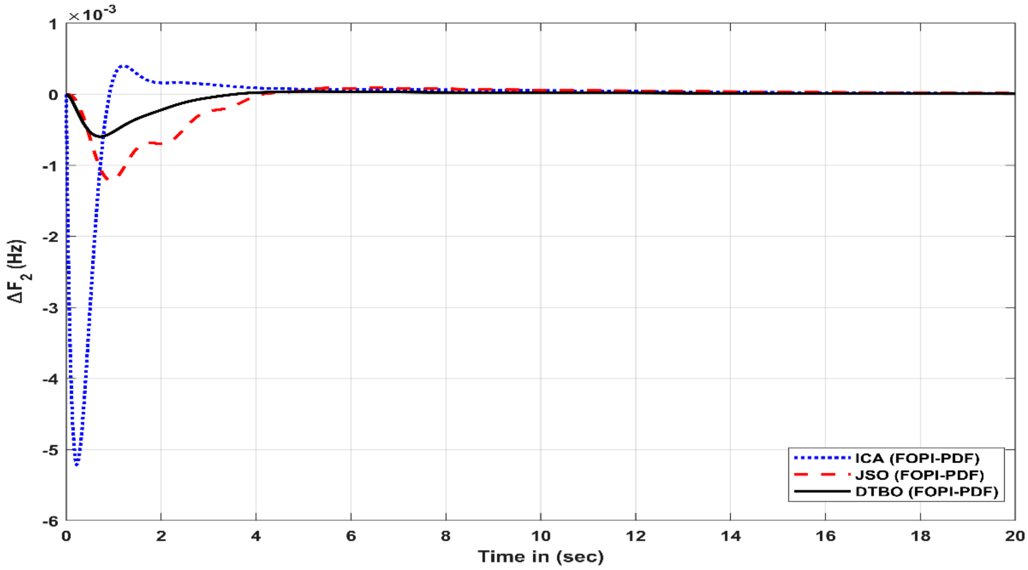

(**b**)

Figure 8. *Cont.*

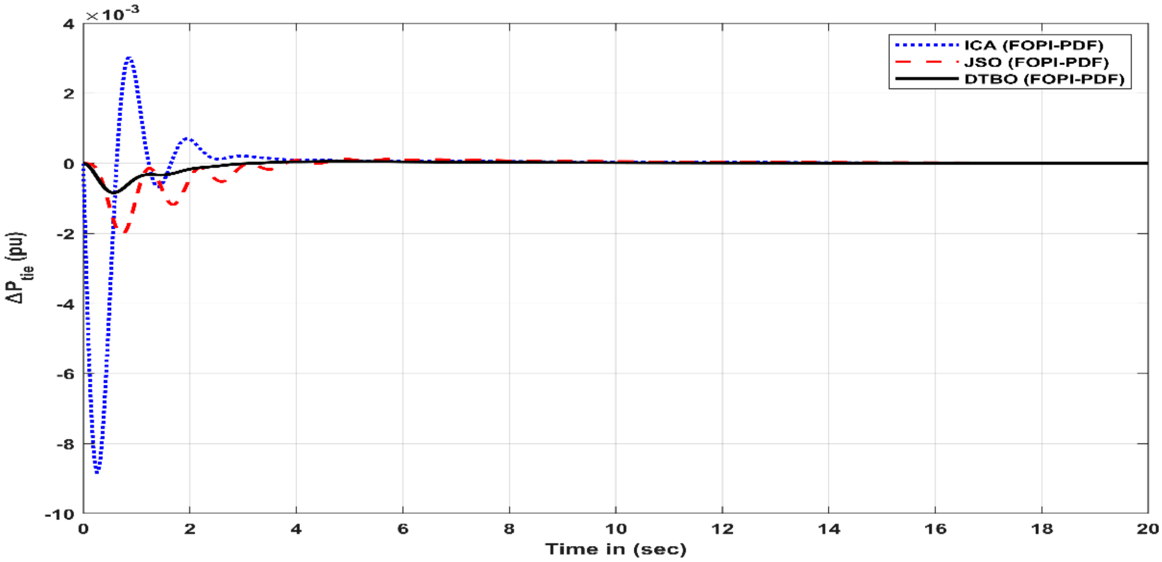

(**c**)

Figure 8. Dynamic response of the power system for case-1 (**a**) ΔF_1 (**b**) ΔF_2 (**c**) ΔP_{tie}.

Table 2. Transient results for PS considering Case-1.

Techniques	**ST (Settling Time)**			**MO (Maximum Overshoot)**			**MU (Minimum Undershoot)**		
	Area 1	**Area 2**	**(ΔP_{tie})**	**Area 1**	**Area 2**	**(ΔP_{tie})**	**Area 1**	**Area 2**	**(ΔP_{tie})**
DTBO: FOPI-PDF	8.23	3.93	2.96	0.000041	0.000272	0.000000	−0.00059	−0.00178	−0.00084
JSO: FOPI-PDF	8.09	9.13	7.83	0.000090	0.000509	0.000127	−0.00121	−0.00500	−0.00202
ICA: FOPI-PDF	10.4	6.44	4.68	0.000402	0.006035	0.003012	−0.00521	−0.01376	−0.00883
[10] hTLBO-PS	13.7	9.53	10.36	0.070400	0.007222	0.003500	−0.24010	−0.18888	−0.06330
[42] hDE-PS	19.0	18.09	12.69	0.00080	0.001700	0.000600	−0.00100	−0.01500	−0.00800
[25] FPA	25.5	23.2	18.77	0.00680	0.01170	0.00260	−0.02450	−0.02288	−0.00440

5.2. Case-2

In this case, the effectiveness of a FOPI-PDF controller using the DTBO technique was compared to the performances of FOPIDF, FOPID, PID, FOTID, and PI controllers. As shown in Figure 9a–c, the dynamic response for each controller has been evaluated for the interconnected tie line (ΔPtie), area 2 (ΔF2), and area 1 (ΔF1). Table 3 shows the overall comparison for various controllers in terms of transient contents, including MO, MU, and ST for (ΔF1), (ΔF2), and (ΔPtie). It is noticeable from Table 3 and Figure 9c that our suggested FOPI-PDF controller (MO = 0.000129, MU = −0.00065) has the least undershoot and overshoot as compared to FOPIDF (MO = 0.000218, MU = −0.00119), PID (MO = 0.000437, MU = −0.00627), PI (MO = 0.001045, MU = −0.00722), MID (MO = 0.000600, MU =−0.00800), and FOTID controller (MO = 0.00260, MU = −0.00440) for interconnected tie-line. It can also be seen from Table 3 and Figure 9c that FOPIDF controllers optimized with DTBO have the lowest settling time for area 1 (ST = 4.420), followed by PID controllers (ST = 5.020), PI controllers (6.533), FOPI-PDF controllers (ST = 8.434), MID controllers (ST = 19.01), and FOTID controllers (ST = 25.5). In a tie-line, the FOPI-PDF controller (ST = 5.98) is very excellent in terms of other controllers, including FOPIDF (ST = 12.60), PID (8.83), PI (ST = 6.82), MID (ST = 12.69), and FOTID (ST = 18.77). Therefore, it is evident from Figure 9c that the current described approach outperforms FOPIDF, PID, PI, and FOTID controllers in terms of ST, MO, and MU for interconnected tie-lines. From Figure 9b, it can also be observed that the PID controller tuned with the DTBO algorithm has superior performance (ST = 6.23) as compared to the FOPIDF controller with (ST = 8.61), the PI controller with (ST = 9.93), the FOPI-PIDF controller with (ST = 10.9), the MID controller with (ST = 18.09), and the FOTID controller with (ST = 23.2).

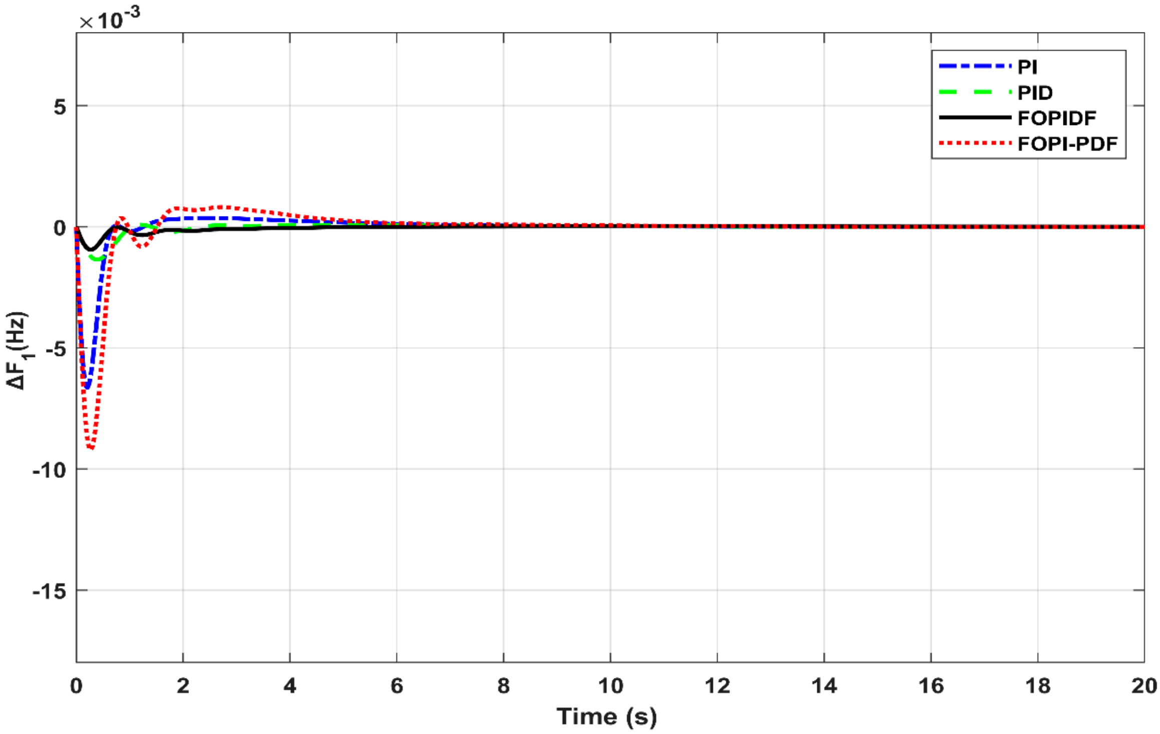

(**a**)

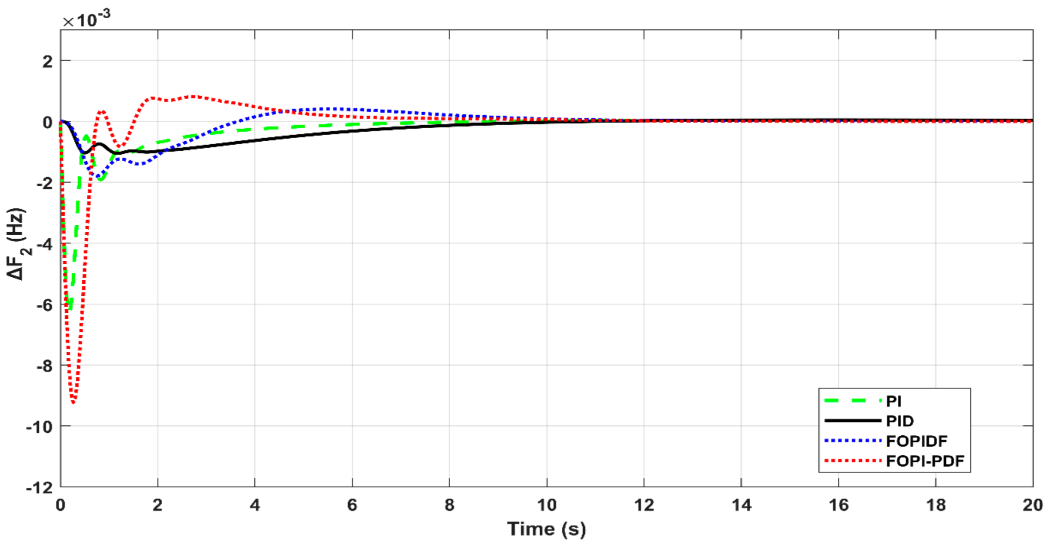

(**b**)

Figure 9. *Cont.*

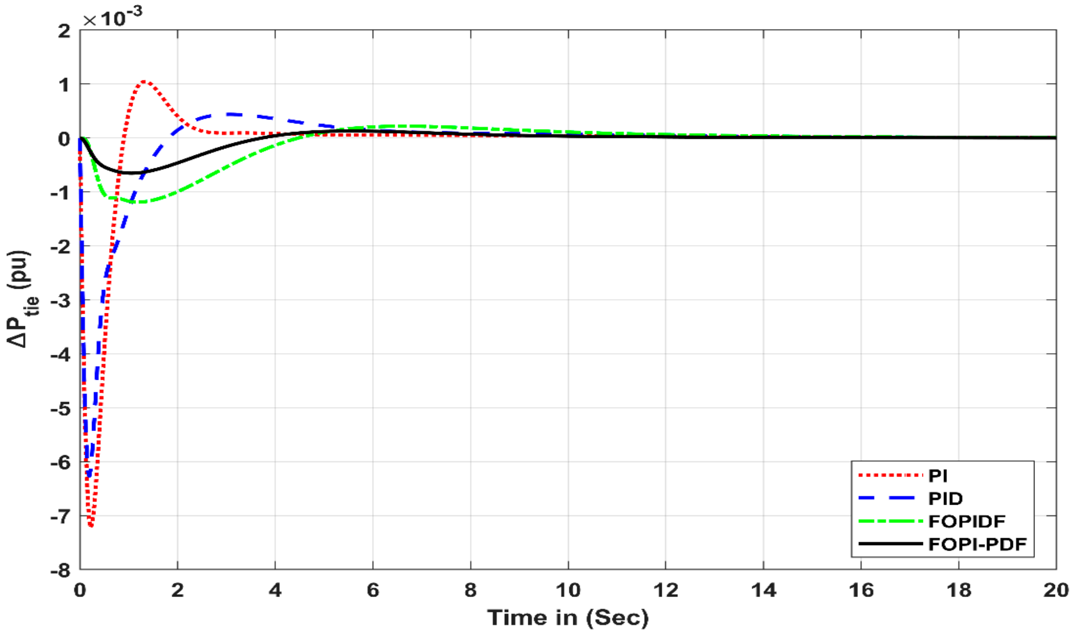

(**c**)

Figure 9. Dynamic response of the PS for Case-2 (**a**) ΔF_1 (**b**) ΔF_2 (**c**) ΔP_{tie}.

Table 3. Transient results for hybrid PS considering Case-2.

Controllers	ST (Settling Time)			MO (Maximum Overshoot)			MU (Minimum Undershoot)		
	Area 1	Area 2	(ΔP_{tie})	Area 1	Area 2	(ΔP_{tie})	Area 1	Area 2	(ΔP_{tie})
FOPI-PDF: DTBO	8.434	10.9	5.98	0.000813	0.000813	0.000129	−0.00922	−0.00922	−0.00065
FOPIDF: DTBO	4.420	8.61	12.6	0.000082	0.000406	0.000218	−0.00135	−0.00179	−0.00119
PID: DTBO	5.020	6.23	8.83	0.000363	0.000048	0.000437	−0.00664	−0.00628	−0.00627
PI:DTBO	6.533	9.93	6.82	0.000017	0.000041	0.001045	−0.00094	−0.00104	−0.00722
[42] MID: hDE-PS	19.01	18.09	12.69	0.00080	0.001700	0.000600	−0.00100	−0.01500	−0.00800
[25] FOTID:FPA	25.5	23.2	18.77	0.00680	0.01170	0.00260	−0.02450	−0.0228	−0.00440

5.3. Case-3

As shown in Figure 10a–c, the convergence curves of various algorithms, including DTBO, ICA, and JSO, have been assessed for hybrid interconnected PS in this case. Using the ITSE assessments as a cost function, the suggested FOPI-PDF controller parameters are fine-tuned. The DTBO parameters listed in Appendix A were selected to yield the best possible controller improvements. There are 30 simulated runs with 80 iterations, and the rest of the parameters are detailed in Appendix B. Each optimization method uses 20 populations. As can be seen in Figure 10a–c, the suggested DTBO optimization procedure outperforms the investigated JSO and ICA optimizers in terms of conversion characteristics for ITSE objective functions. Figure 10a–c demonstrates that, in comparison to JSO and ICA, whose ITSE values are 8.27×10^{-4} and 5.92×3, respectively, the DTBO method converges quickly under ITSE situations and obtains a value of (ITSE = 6.83×10^{-4}).

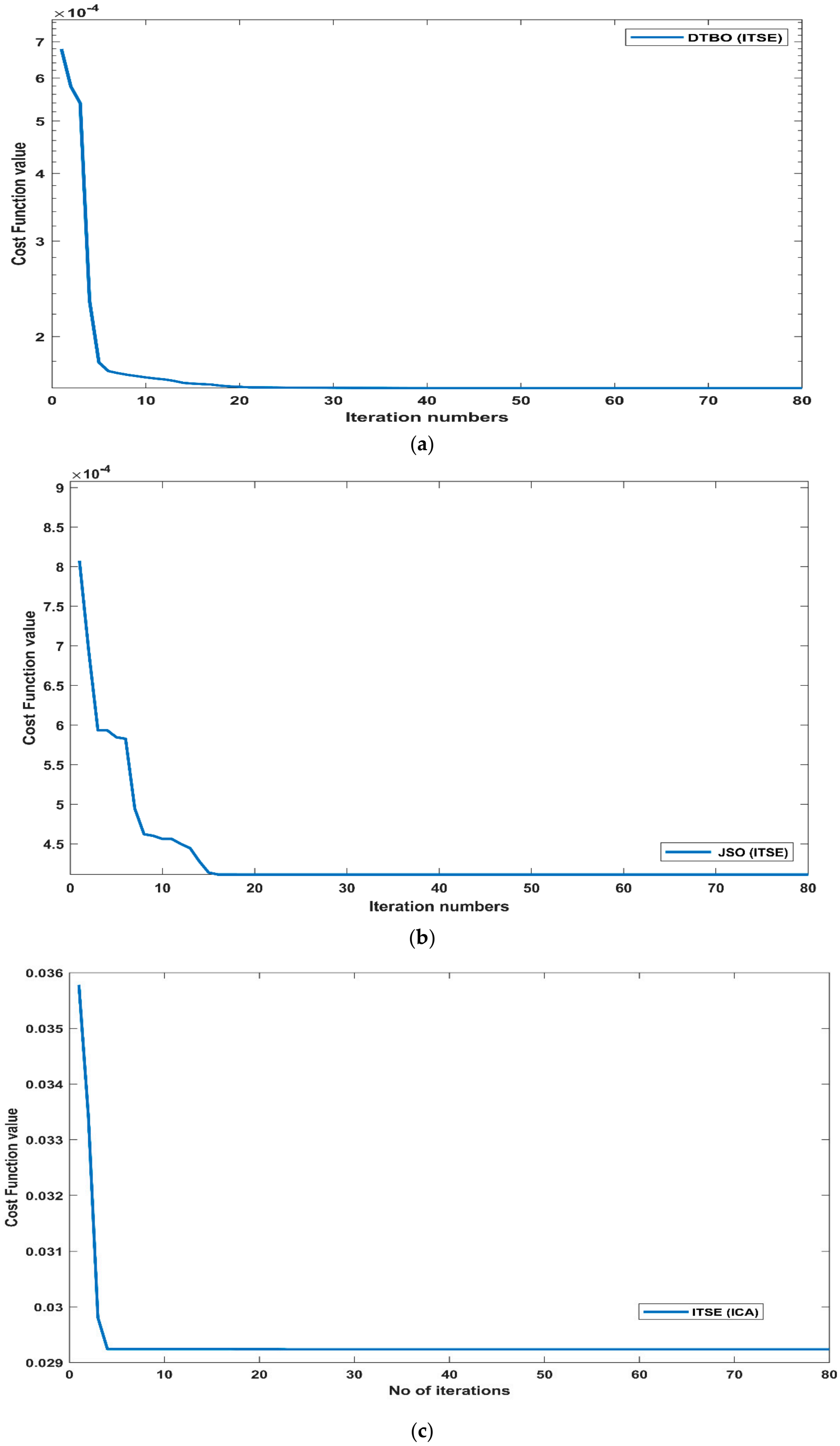

Figure 10. Convergence characteristics curve for algorithms (**a**) DTBO (**b**) JSO (**c**) ICA.

5.4. Sensitivity Analysis/Rubustness

Although system models can be described mathematically in a variety of ways, and because system parameters and configuration might vary over time as a result of the deterioration of system components, the given controller must be robust in the face of parameter uncertainties. Parametric uncertainties in the system can occasionally disrupt stability when the proposed control structure is unable to account for them. Parameters such as Kw, R, Kre, and Tgr are all varied by roughly ±40% from their nominal values and compared to their minimal responses in order to verify the robustness of the proposed controller. Figure 11a–c displays validation of the DTBO: FOPI-PDF controller performance under varying load disturbances up to 25% and ±50%, representing real-world circumstances. Results obtained with varying system parameters are shown in Figure 12 and Table 4, proving the proposed controller's robustness in the face of parameter uncertainty. Furthermore, the load characteristics of a real-world power system are highly unpredictable and varied. The mechanism of control needs to be flexible enough to handle unpredictable changes in load. Consequently, the proposed controller is resilient under a wide range of loads. As can be seen in Table 4, the actual system response is quite close to the nominal values for several parameters. The results show that the proposed DTBO-based FOPI-PDF controller consistently executes within a ± 40% tolerance band for the PS parameters. Furthermore, for a large variety of parameters at the rated value, the suggested controller's optimal values do not necessitate retuning.

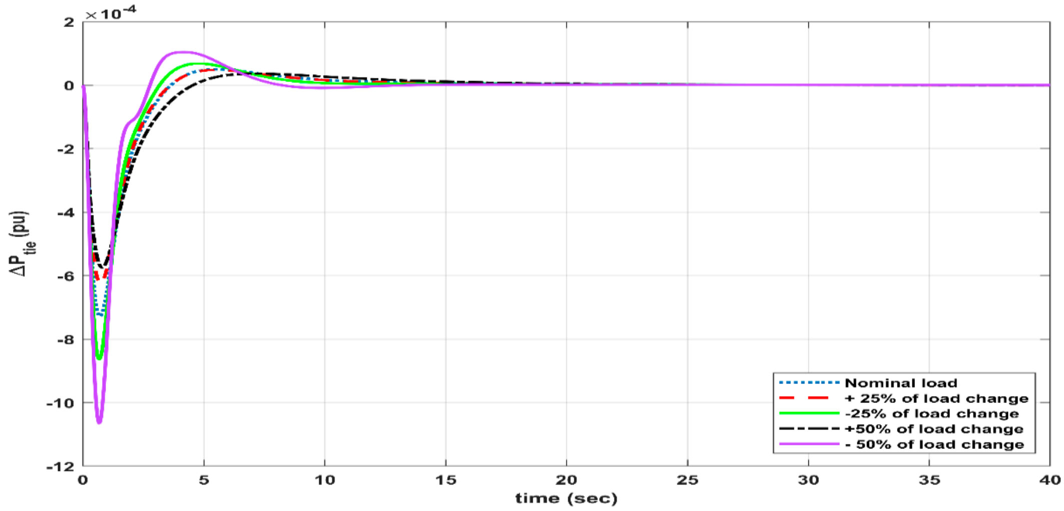

(**a**)

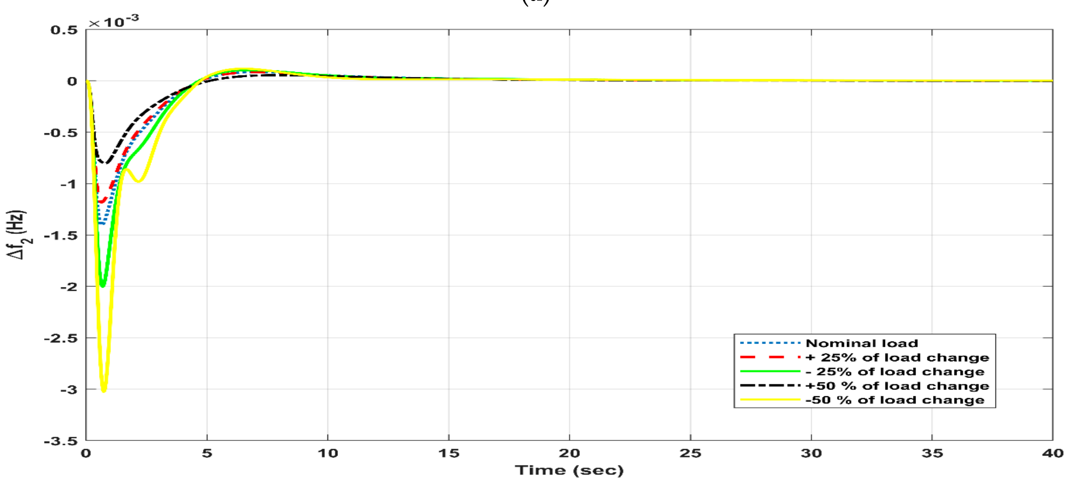

(**b**)

Figure 11. *Cont.*

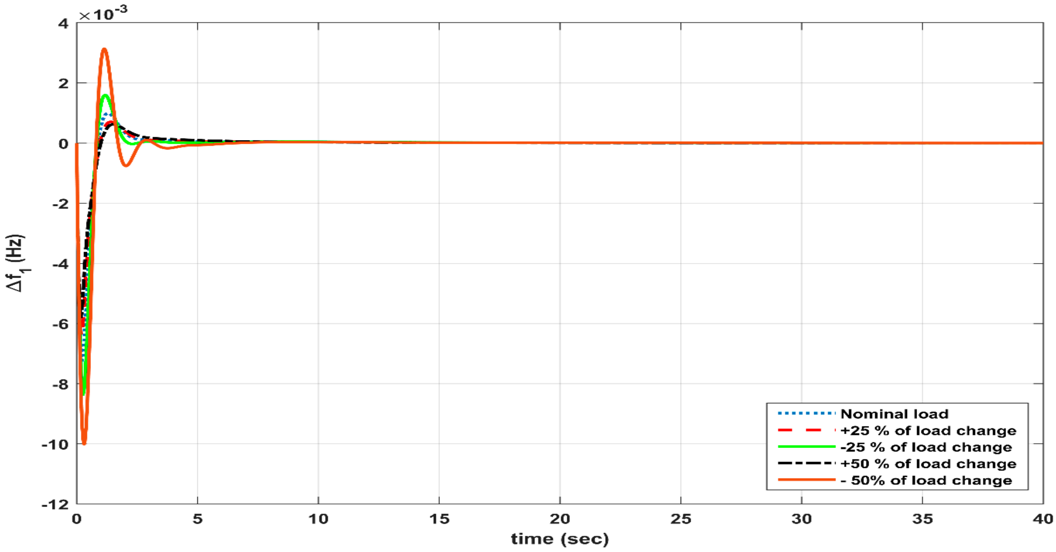

(c)

Figure 11. Different load change for the system considering (**a**) ΔPtie (**b**) ΔF2 (**c**) ΔF3.

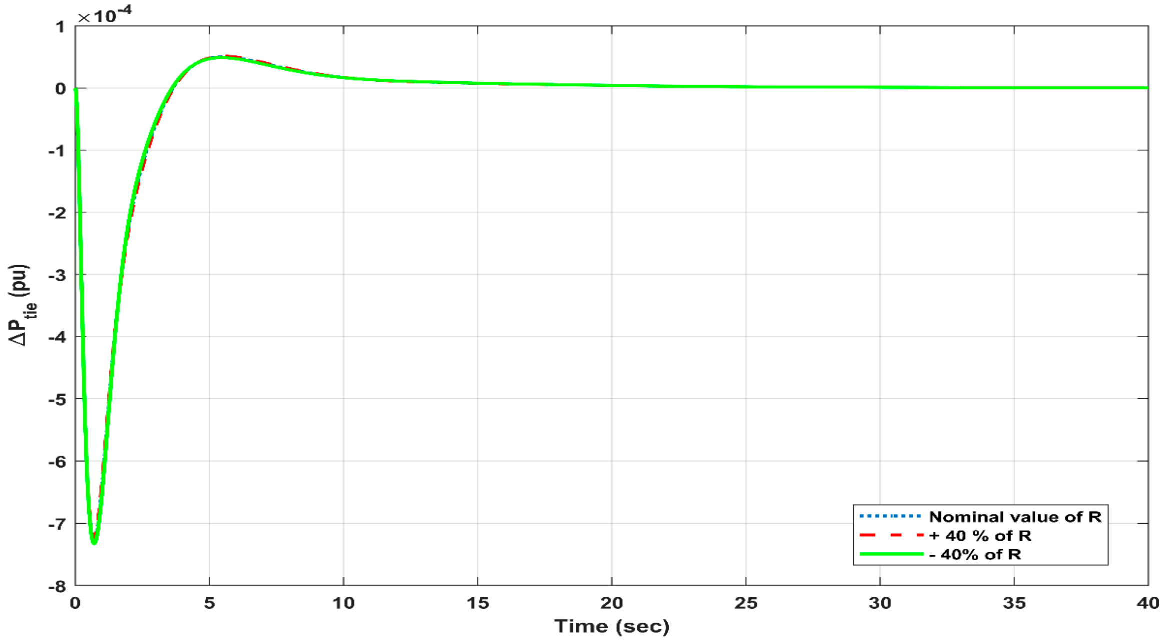

Figure 12. Sensitivity analysis for the system parameters.

Table 4. Transient response computation for change in parameters of the power system.

Parameter	% Change	ST			MO			MU		
		Area 1	Area 1	ΔP_{tie}	Area 1	Area 1	(ΔP_{tie})	Area 1	Area 1	(ΔP_{tie})
K_w	+40	6.09	13.23	14.89	0.00031	0.00032	0.00063	−0.00251	−0.00830	−0.00623
	−40	7.82	13.23	14.90	0.00031	0.00031	0.00061	−0.00257	−0.00840	−0.00618
K_{re}	+40	6.38	13.45	14.21	0.0002	0.00037	0.00094	−0.00489	−0.00713	−0.00693
	−40	8.03	13.46	14.23	0.0002	0.00030	0.00098	−0.00482	−0.00913	−0.00678
R	+40	6.10	12.79	14.60	0.0003	0.00014	0.00083	−0.00361	−0.00780	−0.00731
	−40	7.80	12.80	14.61	0.0003	0.00017	0.00075	−0.00361	−0.00740	−0.00725
T_{gr}	+40	3.47	12.72	14.09	0.0003	0.00068	0.00064	−0.00315	−0.00240	−0.00610
	−40	3.51	12.73	14.10	0.0002	0.00047	0.00054	−0.00313	−0.00236	−0.00600

6. Conclusions

The proposed FOPI-PDN controller for the LFC of two regions, hybrid renewable energies and conventional power sources, with the incorporation of numerous nonlinearities including GDZ, GRL, TD, and BD, was investigated in this research work. The Driver Training Based Optimization (DTBO), an advanced stochastic meta-heuristic algorithm, was used to optimize the settings of the recommended controller. The simulation results show that the DTBO-based tuned FOPI-PDF controller successfully decreases peak overshoot by 89.12%, 83.11%, and 78.10% for area-2, area-1, and link power variation, respectively, while delivering a minimum undershoot of 79.12%, 73.99%, and 90.00% for both areas and link power. Similarly, as compared to the conventional controller, the DTBO-based FOPI-PDF controllers improve the ST by 46.63%, 30.32%, and 14.11% for the load frequencies (ΔF1), (ΔF2), and (ΔPtie), respectively. Finally, the FOPI-PDF controller resilience is tested by deviating from the minimal values for the system parameters. The results show that when the system coefficients or load conditions change, the suggested controller gains are not reset. The efficiency of the DTBO-based FOPI-PDF controller shows that it can successfully manage LFC difficulties in hybrid power systems with protracted oscillations. In the future, the proposed control scheme could be extended to include three or more areas as well as regulation of the combined effect of frequency and voltage for multigeneration interconnected renewable/non-renewable power systems.

Author Contributions: Conceptualization, G.Z. and A.B.; data curation, A.D. and M.I.K.; formal analysis, A.B.; investigation, I.A.K. and M.I.K.; methodology, M.U.; project administration, G.Z.; resources, I.A.K. and M.U.; software, A.D. and A.B.; supervision, G.Z.; validation, G.Z.; writing—original draft, A.D.; writing—review & editing, A.D., I.A.K., M.I.K. and M.U. All authors have read and agreed to the published version of the manuscript.

Funding: This work is supported by the "Young Talent Sub-project of Ningbo Yongjiang Talent Introduction Programme under grant no. 20100859001."

Data Availability Statement: No new data were analyzed or generated in this study. Data sharing is not appropriate to this manuscript.

Conflicts of Interest: The authors declare no conflict of interest.

Appendix A

Table A1. Hybrid PS and Their Parametric Values [27,42,44].

LFC model			
Parameter	Value	Parameter	Value
T_{ps1}	11.49	Kps1	68.97
R_H	2.4	Kps2	68.97
T_{ps2}	11.49	β2	0.4312
R_T	2.4	B1	2.4
Reheat Thermal PS			
K_t	0.54367	T_{tr}	0.3
T_{re}	10	K_{re}	0.3
T_{gr}	0.08		
Parameters and their values for Electric Vehicles			
V_{nom}	364.8	C_{nom}	66.2
R_s	0.074	R_t	0.047
C_t	703.6	RT/F	0.02612
Minimum SOC (in Percentage)	10	Maximum SOC (in Percentage)	95
C_{Batt}	24.15		

Table A1. *Cont.*

Hydro Power System			
T_w	1	T_{rh}	28.749
Kh	0.32586	Tr	5
T_{gh}	0.2		
Renewable energy resources			
Ks	0.5	K_T	1
Ts	1	T_T	0.3
K_{WTG}	1	T_{WTG}	1.5
Boiler Dynamic			
Cb	200	K3	0.92
Trb	0.545	Tf	0.23
Tr	1.4	T_{rh}	28.75
K1	0.85	K2	0.095
T_{1b}	0.545	K1b	0.950

Appendix B

Table A2. DTBO Coefficient and Their Values.

Coefficient	Values	Coefficient	Values	Coefficient	Values	Coefficient	Values
No of Iteration	80	Lower limit (Lb)	−2	No of dimension	7	Coefficient	2
No of Population (Np)	30	Constant (R)	0.05	Random Number (r)	[0, 1]	Coefficient	

References

1. Jan, M.U.; Xin, A.; Abdelbaky, M.A.; Rehman, H.U.; Iqbal, S. Adaptive and Fuzzy PI Controllers Design for Frequency Regulation of Isolated Microgrid Integrated With Electric Vehicles. *IEEE Access* **2020**, *8*, 87621–87632. [CrossRef]
2. Hassan, A.; Aly, M.; Elmelegi, A.; Nasrat, L.; Watanabe, M.; Mohamed, E.A. Optimal Frequency Control of Multi-Area Hybrid Power System Using New Cascaded TID-PI$^{\lambda}$D$^{\mu}$N Controller Incorporating Electric Vehicles. *Fractal Fract.* **2022**, *6*, 548. [CrossRef]
3. Xiao, D.; Chen, H.; Wei, C.; Bai, X. Statistical Measure for Risk-Seeking Stochastic Wind Power Offering Strategies in Electricity Markets. *J. Mod. Power Syst. Clean Energy* **2021**, *10*, 1437–1442. [CrossRef]
4. Gulzar, M.M.; Murawwat, S.; Sibtain, D.; Shahid, K.; Javed, I.; Gui, Y. Modified Cascaded Controller Design Constructed on Fractional Operator 'β' to Mitigate Frequency Fluctuations for Sustainable Operation of Power Systems. *Energies* **2022**, *15*, 7814. [CrossRef]
5. Zhang, P.; Daraz, A.; Malik, S.A.; Sun, C.; Basit, A.; Zhang, G. Multi-resolution based PID controller for frequency regulation of a hybrid power system with multiple interconnected systems. *Front. Energy Res.* **2023**, *10*, 1109063. [CrossRef]
6. Arya, Y. Effect of electric vehicles on load frequency control in interconnected thermal and hydrothermal power systems utilizing CFFOIDF controller. *IET Gener. Transm. Distrib.* **2020**, *14*, 2666–2675. [CrossRef]
7. Zaid, S.A.; Bakeer, A.; Magdy, G.; Albalawi, H.; Kassem, A.M.; El-Shimy, M.E.; AbdelMeguid, H.; Manqarah, B. A New Intelligent Fractional-Order Load Frequency Control for Interconnected Modern Power Systems with Virtual Inertia Control. *Fractal Fract.* **2023**, *7*, 62. [CrossRef]
8. Jia, H.; Li, X.; Mu, Y.; Xu, C.; Jiang, Y.; Yu, X.; Wu, J.; Dong, C. Coordinated control for EV aggregators and power plants in frequency regulation considering time-varying delays. *Appl. Energy* **2018**, *210*, 1363–1376. [CrossRef]
9. Arias, N.B.; Hashemi, S.; Andersen, P.B.; Træholt, C.; Romero, R. Assessment of economic bene_ts for EV owners participating in the primary frequency regulation markets. *Int. J. Electr. Power Energy Syst.* **2020**, *120*, 105985. [CrossRef]
10. Khamari, D.; Sahu, R.K.; Gorripotu, T.S.; Panda, S. Automatic generation control of power system in deregulated environment using hybrid TLBO and pattern search technique. *Ain Shams Eng. J.* **2019**, *11*, 553–573. [CrossRef]
11. Vrdoljak, K.; Peri´c, N.; Petrovi´c, I. Sliding modelbased load-frequency control in power systems. *Electr. Power Syst. Res.* **2010**, *80*, 514–527. [CrossRef]
12. Pan, C.; Liaw, C. An adaptive controller for power system load-frequency control. *IEEE Trans. Power Syst.* **1989**, *4*, 122–128. [CrossRef]

13. Arya, Y.; Kumar, N. BFOA-scaled fractional order fuzzy PID controller applied to AGC of multi-area multi-source electric power generating systems. *Swarm Evol. Comput.* **2017**, *32*, 202–218. [CrossRef]
14. Sahu, R.K.; Panda, S.; Biswal, A.; Sekhar, G.C. Design and analysis of tilt integral derivative controller with filter for load frequency control of multi-area interconnected power systems. *ISA Trans.* **2016**, *61*, 251–264. [CrossRef]
15. Malik, S.; Suhag, S. A Novel SSA Tuned PI-TDF Control Scheme for Mitigation of Frequency Excursions in Hybrid Power System. *Smart Sci.* **2020**, *8*, 202–218. [CrossRef]
16. Elmelegi, A.; Mohamed, E.A.; Aly, M.; Ahmed, E.M.; Mohamed, A.A.A.; Elbaksawi, O. Optimized Tilt Fractional OrderCooperative Controllers for Preserving Frequency Stability in Renewable Energy-Based Power Systems. *IEEE Access* **2021**, *9*, 8261–8277. [CrossRef]
17. Arya, Y. A new optimized fuzzy FOPI-FOPD controller for automatic generation control of electric power systems. *J. Frankl. Inst.* **2019**, *356*, 5611–5629. [CrossRef]
18. Paliwal, N.; Srivastava, L.; Pandit, M. Application of grey wolf optimization algorithm for load frequency control in multi-source single area power system. *Evol. Intell.* **2020**, *15*, 563–584. [CrossRef]
19. Ayas, M.S.; Sahin, E. FOPID controller with fractional filter for an automatic voltage regulator. *Comput. Electr. Eng.* **2021**, *90*, 106895. [CrossRef]
20. Yousri, D.; Babu, T.S.; Fathy, A. Recent methodology-based Harris Hawks optimizer for designing load frequency control incorporated in multi-interconnected renewable energy plants. *Sustain. Energy Grids Netw.* **2020**, *22*, 100352. [CrossRef]
21. Daraz, A.; Malik, S.A.; Azar, A.T.; Aslam, S.; Alkhalifah, T.; Alturise, F. Optimized Fractional Order Integral-Tilt Derivative Controller for Frequency Regulation of Interconnected Diverse Renewable Energy Resources. *IEEE Access* **2022**, *10*, 43514–43527. [CrossRef]
22. Oshnoei, A.; Khezri, R.; Muyeen, S.M.; Oshnoei, S.; Blaabjerg, F. Automatic Generation Control Incorporating Electric Vehicles. *Electr. Power Components Syst.* **2019**, *47*, 720–732. [CrossRef]
23. Magdy, G.; Bakeer, A.; Nour, M.; Petlenkov, E. A new virtual synchronous generator design based on the SMES system for frequency stability of low-inertia power grids. *Energies* **2020**, *13*, 5641. [CrossRef]
24. Arya, Y. Impact of ultra-capacitor on automatic generation control of electric energy systems using an optimal FFOID controller. *Int. J. Energy Res.* **2019**, *43*, 8765–8778. [CrossRef]
25. Priyadarshani, S.; Subhashini, K.R.; Satapathy, J.K. Path finder algorithm optimized fractional order tilt-integral-derivative (FOTID) controller for automatic generation control of multi-source power system. *Microsyst. Technol.* **2020**, *27*, 23–35. [CrossRef]
26. Daraz, A.; Malik, S.A.; Basit, A.; Aslam, S.; Zhang, G. Modified FOPID Controller for Frequency Regulation of a Hybrid Interconnected System of Conventional and Renewable Energy Sources. *Fractal Fract.* **2023**, *7*, 89. [CrossRef]
27. Arya, Y. Impact of hydrogen Aqua electrolyzer-fuel cell units on automaticgeneration control of power systems with a new optimal fuzzy TIDFII controller. *Renew. Energy* **2019**, *139*, 468–482. [CrossRef]
28. Mohamed, E.A.; Aly, M.; Watanab, M. New Tilt Fractional-Order Integral Derivative with Fractional Filter (TFOIDFF)Controller with Artificial Hummingbird Optimizer for LFC in Renewable Energy Power Grids. *Mathematics* **2022**, *10*, 3006. [CrossRef]
29. Hasanien, H.M.; El-Fergany, A.A. Salp swarm algorithm-based optimal load frequency control of hybrid renewable power systems with communication delay and excitation cross-coupling effect. *Electr. Power Syst. Res.* **2019**, *176*, 105938. [CrossRef]
30. Latif, A.; Hussain, S.M.S.; Das, D.C.; Ustun, T.S. Optimum synthesis of a BOA optimized novel dual-stage PI-(1 C ID) controller for frequency response of a microgrid. *Energies* **2020**, *13*, 3446. [CrossRef]
31. Arya, Y.; Kumar, N.; Dahiya, P.; Sharma, G.; Çelik, E.; Dhundhara, S.; Sharma, M. Cascade-IDN controller design for AGC of thermal and hydro-thermal power systems integrated with renewable energy sources. *IET Renew. Power Gener.* **2020**, *15*, 504–520. [CrossRef]
32. Khamies, M.; Magdy, G.; Selim, A.; Kamel, S. An improved Rao algorithm for frequency stability enhancement of nonlinearpower system interconnected by AC/DC links with high renewables penetration. *Neural Comput. Appl.* **2021**, *34*, 2883–2911. [CrossRef]
33. Ali, H.H.; Fathy, A.; Kassem, A.M. Optimal model predictive control for LFC of multi-interconnected plants comprising renewable energy sources based on recent sooty terns approach. *Sustain. Energy Technol. Assess.* **2020**, *42*, 100844. [CrossRef]
34. Dehghani, M.; Trojovská, E.; Trojovský, P. A new human-based metaheuristic algorithm for solving optimization problems on the base of simulation of driving training process. *Sci. Rep.* **2022**, *12*, 9924. [CrossRef]
35. Gulzar, M.M.; Iqbal, A.; Sibtain, D.; Khalid, M. An Innovative Converterless Solar PV Control Strategy for a Grid Connected Hybrid PV/Wind/Fuel-Cell System Coupled with Battery Energy Storage. *IEEE Access* **2023**, *11*, 23245–23259. [CrossRef]
36. Yakout, A.H.; Kotb, H.; Hasanien, H.M.; Aboras, K.M. Optimal Fuzzy PIDF Load Frequency Controller for Hybrid Microgrid System Using Marine Predator Algorithm. *IEEE Access* **2021**, *9*, 54220–54232. [CrossRef]
37. Yousri, D.; Babu, T.S.; Beshr, E.; Eteiba, M.B.; Allam, D. A robust strategy based on marine predators algorithm for large scale photovoltaic array reconguration to mitigate the partial shading effect onthe performance of PV system. *IEEE Access* **2020**, *8*, 112407–112426.
38. Elkasem, A.H.A.; Kamel, S.; Hassan, M.H.; Khamies, M.; Ahmed, E.M. An Eagle Strategy Arithmetic Optimization Algorithm for Frequency Stability Enhancement Considering High Renewable Power Penetration and Time-Varying Load. *Mathematics* **2022**, *10*, 854. [CrossRef]
39. Ahmed, E.M.; Mohamed, E.A.; Elmelegi, A.; Aly, M.; Elbaksawi, O. Optimum Modified Fractional Order Controller for FutureElectric Vehicles and Renewable Energy-Based Interconnected Power Systems. *IEEE Access* **2021**, *9*, 29993–30010. [CrossRef]

40. Ali, T.; Malik, S.A.; Daraz, A.; Aslam, S.; Alkhalifah, T. Dandelion Optimizer-Based Combined Automatic Voltage Regulation and Load Frequency Control in a Multi-Area, Multi-Source Interconnected Power System with Nonlinearities. *Energies* **2022**, *15*, 8499. [CrossRef]
41. Mohamed, E.A.; Ahmed, E.M.; Elmelegi, A.; Aly, M.; Elbaksawi, O.; Mohamed, A.A.A. An Optimized Hybrid Fractional Order Controller for Frequency Regulation in Multiarea Power Systems. *IEEE Access* **2020**, *8*, 213899–213915. [CrossRef]
42. Sahu, R.; Gorripotu, T.; Panda, S. A hybrid DE-PS algorithm for load frequency control under deregulated power system withUPFC and RFB. *Ain Shams Eng. J.* **2015**, *6*, 893–911. [CrossRef]
43. Tasnin, W.; Saikia, L.C.; Raju, M. Deregulated AGC of multi-area system incorporating dish-Stirling solar thermal and geothermalpower plants using fractional order cascade controller. *Int. J. Electr. Power Energy Syst.* **2018**, *101*, 60–74. [CrossRef]
44. Ahmed, E.M.; Selim, A.; Alnuman, H.; Alhosaini, W.; Aly, M.; Mohamed, E.A. Modified Frequency Regulator Based on TI$^{\lambda}$-TD$^{\mu}$FF Controller for Interconnected Microgrids with Incorporating Hybrid Renewable Energy Sources. *Mathematics* **2023**, *11*, 28. [CrossRef]
45. Micev, M.; Calasan, M.; Oliva, D. Fractional Order PID Controller Design for an AVR System Using Chaotic Yellow Saddle Goatfish Algorithm. *Mathematics* **2020**, *8*, 1182. [CrossRef]